ADVANCED MATERIALS

[10] For a discussion of radical-radical couplings and radical cation electrophilic substitution pertinent to thiophene polymerizations, see: Y. Wei, C.-C. Chan, J. Tian, G.-W. Jang, K. F. Hsueh, *Chem. Mater.* **1991**, *3*, 888.
[11] In studies of non-polymerizable pendant thienyl monomers having blocking groups in the 5-thienyl position, we have observed single low potential chemical cyclization waves that exhibit complete irreversibility followed by single stable, reversible redox couples with peak anodic potentials slightly higher than that for the preceding chemical step. In the absence of blocking substituents at the reactive ring positions, these naphthodithiophene radical cations polymerize.
[12] For recent work employing $FeCl_3$ oxidation to effect arene–arene cyclizations in large oligophenylenes, see: F. Dötz, J. D. Brand, S. Ito, L. Gherghel, K. Müllen, *J. Am. Chem. Soc.* **2000**, *122*, 7707.
[13] J. L. Brédas, *J. Chem. Phys.* **1985**, *82*, 3808.
[14] T. R. Kelly, Q. Li, V. Bhushan, *Tetrahedron Lett.* **1990**, *31*, 161.
[15] K. Sonogashira, Y. Tohda, N. Hagihara, *Tetrahedron Lett.* **1975**, 4467.
[16] T. Sauer, G. Wegner, *Mol. Cryst. Liq. Cryst. B* **1988**, *162*, 97.
[17] W. T. Ford, L. Sumner, W. Zhu, Y. H. Chang, P.-J. Um, K. H. Choi, P. A. Heiney, N. C. Maliszewskyj, *New J. Chem.* **1994**, *18*, 495.
[18] Q. Zhou, P. J. Carroll, T. M. Swager, *J. Org. Chem.* **1994**, *59*, 1294.

Nanoscale Lateral Field-Emission Triode Operating at Atmospheric Pressure**

By *Laura Pescini*, *Armin Tilke*, *Robert H. Blick*,* *Heribert Lorenz*, *Jörg P. Kotthaus*, *Werner Eberhardt*, and *Dieter Kern*

Silicon-based transistors are state of the art amplifiers and only the true admirers of hifi electronics are still using tube based amplifiers, appreciating the clear sound these produce. Nevertheless, even vacuum tubes in monitors and television sets might soon be outperformed by field-emission devices in flat panel displays, which are also seen as the most promising challenge to liquid crystal displays (LCDs).[1] The main reasons for this are the very low operation voltages and, if silicon is used as the starting material, the low cost and the possibility to integrate the field-emitters in current silicon technology.[2] Commonly, field-emission devices machined on the 10 nm scale are limited to low pressures down to 10^{-9} mbar,[3] much like conventional electron tubes. Nevertheless, in recent work by Driskill-Smith et al.,[4] effective functioning of nanoscale field-emitters at atmospheric pressure was demonstrated.

The underlying idea for the device we fabricated is a combination of well-established silicon nanotechnology and of the principle of a triode amplifier. We show how this device functions as a classical triode on the nanometer scale and, resulting from the small dimensions, how it is operated under ambient pressure at room temperature. The gating allows to direct the electron current and amplify it locally with low power consumption. Typical operating voltages of the device are of the order of only 2 V, which makes it suitable for low-power electronics.

The material of choice for such three-dimensional nanosculpturing is silicon-on-insulator (SOI). The SOI wafers are highly n-doped by phosphorus diffusion from a solid dopant source. The silicon film has a thickness of 190 nm and the buried oxide (BOX) is around 360 nm. In transport measurements the doping level turned out to be about 5×10^{19} cm^{-3}. The triode structure is defined by high-resolution low-energy electron-beam lithography using a two-layer positive electron resist, namely poly(methylmethacrylate) (PMMA). A 30 nm aluminum film is evaporated to serve as an etch mask in the following reactive ion etching of the silicon film, which is performed using CF_4. Undercutting of the defined structures is achieved by removing the BOX in an etchant with a 49:1 volume ratio of H_2O/HF (water and hydrofluoric acid). The aluminum layer itself is simultaneously removed by the HF solution. Since the silicon is highly doped, this etching process also leads to an effective shrinking of the electrodes with an etch rate of about 1.8 nm/min.[5] After removing the sacrificial layer, the triodes are finally suspended in a critical point dryer in order to avoid lift-off of the triode structure by the surface tension of the solvents. The suspended silicon nanostructure is shown in Figure 1.

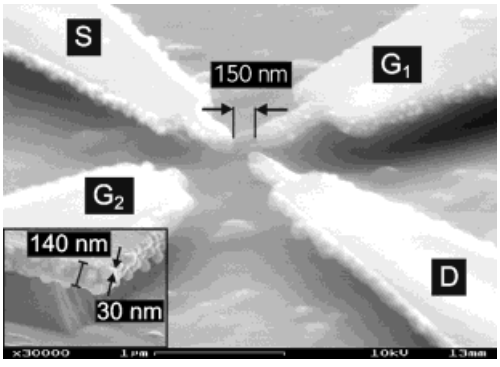

Fig. 1. Scanning electron micrograph of the free-standing silicon nanostructure: Aerial view of the device with the contacts marked as source (S), drain (D), gate 1 (G_1), and gate 2 (G_2). Inset: Silicon/phosphorus grains with sizes on the order of 10–30 nm are found on the edges of the doped substrate, constituting the field-emission tips.

We use a typical current measurement setup with low-noise preamplifiers and common voltage sources. This enables monitoring of drain and gate currents simultaneously. Most of the measurements are performed in a sample holder at room temperature, allowing the flow of different coupling gases. The devices we designed are set up much like a classical triode tube amplifier, as seen in Figure 1. The leads are completely undercut, thus inhibiting current flow across the substrate. The gate electrodes are aligned perpendicularly to source (S) and drain (D) contacts. This convention is adopted for the

[*] Dr. R. H. Blick, L. Pescini, Dr. A. Tilke, Dr. H. Lorenz, Prof. J. P. Kotthaus
Center for NanoScience and Sektion Physik
Ludwig-Maximilians-Universität
Geschwister-Scholl-Platz 1, D-80539 München (Germany)
E-mail: robert.blick@physik.uni-muenchen.de
Dr. W. Eberhardt, Prof. D. Kern
Institut für Angewandte Physik, Universität Tübingen
Auf der Morgenstelle 10, D-72076 Tübingen (Germany)

[**] We acknowledge technical support by A. Kriele and S. Manus. The SOI-wafers were donated by Siemens AG, Munich. We acknowledge financial support from the German ministry of science (BMBF) under contract number 01M2413C6 and the Deutsche Forschungsgemeinschaft (project: Bl/487–2).

  0935-9648/01/2312-1780 $ 17.50+.50/0

sake of clarity only, since a current flow is possible in the device between each of the four contacts, as will be shown later. The distance between the S/D electrodes is chosen to be around 190 nm. The two gates, G_1 and G_2, are defined at distances of 150 nm and 300 nm from the electron path, respectively. The aim of this arrangement is to study the influence of local electric field gradients on the functioning of the triode. The proximity of the gates ensures that the electrons suffer few scattering events only, assuming an elastic mean free path of 200 nm.[6] Electrons are emitted from nanometer-sized silicon/phosphorus grains with typical radii of curvature of only some 10 nm, which are found on the electrodes surface (presumably caused by the dry etching process).[7] These grains are shown in a close-up of an undercut device edge in the inset of Figure 1. The inset also shows the 360 nm thick SiO_2 layer, which is located between the active device and the substrate. This BOX provides electrical insulation, eliminating the possibility of conducting paths through the substrate. The substrate itself was grounded during the measurements. In control measurements we also verified the current flowing between the top electrodes and the substrate, which turned out to be about 0.3 pA at an applied voltage of 4 V. This is three orders of magnitude below the field-emitter current and can be neglected. Comparing our structure with field-emitters fabricated by electron-beam induced deposition,[8–10] we find similar radii of curvature but considerably smaller operating voltages, although supertips prepared with the deposition technique show much higher emission currents.[11]

The work function Φ of an ideal clean and well oriented silicon surface under flatband conditions in ultra high vacuum is about 4.5 eV. It is defined as the minimum energy that an electron at the Fermi level must possess to escape into vacuum, and is given by

$$\Phi = e\chi + \frac{E_g}{2} + e\Psi \tag{1}$$

where e is the electron charge, χ is the electron affinity, E_g is the energy gap, and Ψ is the potential difference between the Fermi level and the intrinsic level.[12] Intrinsic or defect induced surface states lead to band bending and therefore to a change in Ψ. The high doping level of the silicon tips used here gives a value of $\Psi \sim -0.6$ V. Moreover, the adsorption (physisorption or chemisorption) of atoms or molecules such as water, oxygen, or hydrogen can reduce the electron affinity so far, that the vacuum level comes close to the conduction band minimum.[13] In our case the strong doping leads to the formation of phosphorus precipitates with an effective work function of the order of 1.5–2.0 eV,[14] which explains the low turn-on voltage observed (see below).

Cold field emission from a metallic surface can be described by the Fowler–Nordheim equation. The main underlying assumptions are a smooth flat metallic surface, a uniform work function across the surface and the possibility to describe the interaction between the emitted electrons and the metallic surface by an image potential. The so-called elementary Fowler–Nordheim equation neglects the reduction of the potential wall near the metallic surface caused by the image potential. In this approximation, the equation is given by[15]

$$I = Aa\frac{1}{\Phi}F^2 \exp\left(\frac{-b\Phi^{\frac{3}{2}}}{F}\right) \tag{2}$$

with

$$a = \frac{e^3}{8\pi h} \approx 1.54 \times 10^{-6}\frac{AeV}{V^2} \tag{3}$$

$$b = \frac{8\pi\sqrt{2me}}{3eh} \approx 6.83 \times 10^9 eV^{-\frac{3}{2}}\frac{V}{m} \tag{4}$$

where h is Planck's constant, A is the emission area, m is the electron mass, and F the local electric field at the surface. If any of the above mentioned conditions is not satisfied, Equation 2 is modified by introducing two correction factors λ and μ.[16] This leads to the so-called generalized Fowler–Nordheim equation

$$I = \lambda Aa\frac{1}{\Phi}F^2 \exp\left(\frac{-\mu b\Phi^{\frac{3}{2}}}{F}\right) \tag{5}$$

Since it is extremely difficult to determine the local electric fields in the nano-triode, application of Equation 5 is limited. Nevertheless, a linear expression is usually sufficient

$$F = kV \tag{6}$$

In order to fit the experimentally obtained data with Equation 5 the following form is used

$$I = \alpha V^2 e^{-\beta/V} \tag{7}$$

where α and β are fit parameters and I is the measured current.

Figure 2 shows the I–V-curve of the nano-triode measured. The suspended field-emitter exhibits a very low turn-on voltage (compared, e.g., to Driskill-Smith et al.[16]) of about 1.5 V

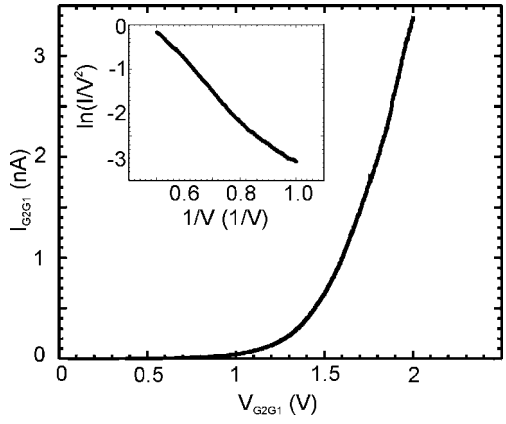

Fig. 2. I–V characteristic measured between the contacts G_1 and G_2 at $p = 1$ atm and 300 K. The bias on the other electrodes is set to zero ($V_{DS} = 0$) in this case. The inset shows a Fowler–Nordheim plot of $\ln(I/V^2)$ vs. $1/V$.

  0935-9648/01/2312-1781 $ 17.50+.50/0

ADVANCED MATERIALS

with a current level of 1–4 nA, due to the phosphorus precipitates. In this case we measured the current $I_{G_1G_2}$ flowing through the contacts G_1 and G_2 for $V_{DS} = 0$. By fitting the trace in Figure 2, we find: $\alpha \sim 20.74$ nA/V^2 and $\beta \sim 6.34$ V. In order to obtain a value for k in Equation 6 and compare the measurements with the values predicted by Equations 2 and 5, we derive the electric field at the surface of a metallic sphere with 20 nm diameter located at a distance 600 nm from a similar metallic sphere and find $k \sim 0.5 \times 10^8$ m^{-1}. Inserting that value in Equation 7 and comparing the results with Equation 5 using a work function of the order of 2 eV one finds $\lambda A \sim 3 \times 3$ nm^2, a value in reasonable agreement with the geometry of the silicon/phosphorus grains. Regarding Equation 5 one calculates $b\Phi^{3/2}/k \sim 380/\mu$ V; taking into account the conditions required to apply Equations 2 and 5 stated above, this result is also in reasonable agreement with the experimental finding of $\beta \sim 6.34$ V. The inset in Figure 2 shows a typical Fowler–Nordheim plot of $\ln(I/V^2)$ vs. $1/V$. For another field emitting sample we find $\alpha \sim 13.7$ nA/V^2 and $\beta \sim 24.1$ V. From this we obtain $\lambda A \sim 2.5 \times 2.5$ nm^2 and $b\Phi^{3/2}/k \sim 358/\mu$ V.

The main advantage of the nano-triode compared to a common field-emission device is the tunability. To demonstrate this additional flexibility of the nano-triode, we recorded the drain current I_D for different gate voltages. As seen in Figure 3a, where the bias V_{G_1D} is indicated, I_D can be strongly varied by applying a sufficiently large negative voltage V_{G_1D} to the gate G_1 (drain terminal is grounded). We observe a peak structure for $V_{G_1D} \geq -0.75$ V and a broad region of negative differential conductivity. We explain this behavior by considering that, besides the emission from the terminal S (towards D, current indicated as I_{DS}), additional electrons are emitted from the terminal G_1 (towards D, current indicated as I_{G_1D}) when set on a negative potential with respect to the contact D, leading to an increase in the measured total current $I_D = I_{DS} + I_{G_1D}$. For larger values of V_{DS}, however, the contact is negatively biased with respect to the gate G_1 leading to an emission of electrons from S to G_1 and therefore to a decrease of the number of electrons directed towards the drain terminal where the current I_D is measured.

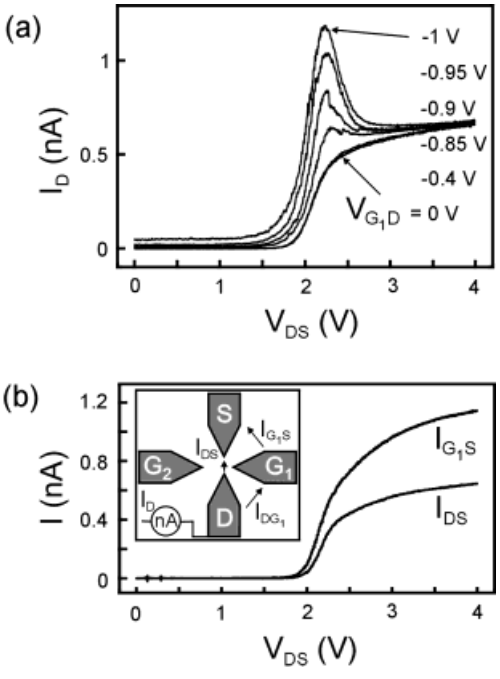

Fig. 3. a) I_D vs. V_{DS} for different gate voltages V_{G_1D} is shown, representing the effective gating of the current (G_2 is grounded). b) The current into gate contact I_{G_1S} is compared to I_{DS}, with $V_{G_1D} = -0.6$ V and G_2 grounded. The two currents are measured simultaneously. The inset shows a schematic plot of the sample with the notation given to the contacts and to the currents.

In Figure 3b we show the simultaneous measurement of I_{DS} and I_{G_1S}. The G_2 terminal is grounded and $V_{G_1D} = -0.6$ V, therefore, as mentioned above, the current I_{DS} does not show any peak structure. Since I_{G_1S} is larger than I_{DS}, according to the lower tip to tip distance, the strong influence of the gate potential in Figure 3a can be understood. In both measurements presented in Figure 3 we observe a saturation of the emitted current for the highest voltages applied. This negative curvature of the Fowler–Nordheim plot indicates a suppression of the electric field at the cathode due to space charge effects, as analyzed in detail by Jensen et al.[7,17] When the collecting mechanism is not efficient, the electric field at the emitter is suppressed by the presence of emitted electrons between cathode and anode. Since the emitted current depends exponentially on the electric field at the emitter tip, even a small decrease of this field strength leads to a saturation of the measured current.

As mentioned above we assume that the electrons are emitted from the source contact. Since their mean free path in air is around 200 nm and the typical electrode distances are 150 nm, most of the electrons follow a straight trajectory only deflected by the gate electrodes. This assumption is also supported by comparing different coupling gases. In Figure 4 we show the results of the measurements in which we operate the triode in ^{4}He at $p \sim 10^{-2}$ mbar, N_2 at 10^{-2} mbar, in vacuum at 10^{-6} mbar, and in air at ambient pressure (traces are offset

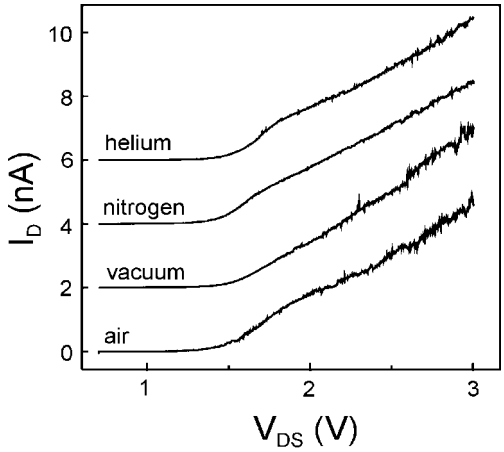

Fig. 4. The drain current I_D vs. voltage V_{DS} applied between drain and source terminals of the nano-triode is shown for different coupling gases in the sample holder and $V_{G_1,2}D = -0.6$ V (traces are offset for clarity). Note the almost identical slopes and turn-on voltages for all gases used.

  0935-9648/01/2312-1782 $ 17.50+.50/0

for clarity). The gate voltages are set to $V_{G_1D} = V_{G_2D} = -0.6$ V, therefore $I_{G_2D} \geq 0$ and I_D is enhanced. Moreover, setting $V_{G_1D} = V_{G_2D} = -0.6$ V, an extractor field is created which acts on the drain electrode, resulting in an improved collection mechanism, which prevents the formation of a space charge region, thus no saturation is observed.

As can be seen, the general behavior is reproduced in all four cases, i.e., we find similar turn-on voltages and slopes of the *I–V*-characteristics. This is a clear indication that possible electron scattering does not lead to gas ionization. Finally, it should be noted that the device was continuously operated for several weeks without severe degradation effects.

In conclusion we demonstrated the functioning of a nano-triode, an integrated fully tunable field-emitter, fabricated out of doped SOI material. This lateral nano-triode operates at room temperature and under ambient pressure. The main advantages of this approach are low turn-on voltages and the possibility of direct integration into existing silicon technology. Within this setup it is possible to tune the current collected at the drain electrode by biasing the gate electrodes. Work is in progress to improve the performance and especially the amplification of the device.

Received: May 2, 2001
Final version: August 2, 2001

[1] D. Temple, W. D. Palmer, L. N. Yadon, J. E. Mancusi, D. Vellenga, G. E. McGuire, *J. Vac. Sci. Technol. A* **1998**, *16*, 1980.
[2] B. Wang, L. Tong, J. K. O. Sin, V. M. C. Poon, *J. Vac. Sci. Technol. B* **1996**, *14*, 1938.
[3] N. S. Xu, J. C. She, S. E. Huq, J. Chen, S. Z. Deng, *Appl. Phys. Lett.* **1998**, *73*, 3668.
[4] A. A. G. Driskill-Smith, D. G. Hasko, H. Ahmed, *Appl. Phys. Lett.* **1997**, *71*, 3159. A. A. G. Driskill-Smith, D. G. Hasko, H. Ahmed, *J. Vac. Sci. Technol. B* **1997**, *15*, 2773.
[5] L. Pescini, A. Tilke, R. H. Blick, H. Lorenz, J. P. Kotthaus, W. Eberhardt, D. Kern, *Nanotechnology* **1999**, *10*, 418. L. Pescini, *Diploma Thesis*, Ludwig-Maximilians-Universität München and Università degli Studi di Firenze, **1999**.
[6] T. K. S. Wong, S. G. Ingram, *J. Phys. D* **1993**, *26*, 979.
[7] K. L. Jensen, J. E. Yater, E. G. Zaidman, M. A. Kodis, A. Shih, *J. Vac. Sci. Technol. B* **1998**, *16*, 2038.
[8] M. Weber, M. Rudolph, J. Kretz, H. W. P. Koops, *J. Vac. Sci. Technol. B* **1995**, *13*, 461.
[9] H. W. P. Koops, C. Schössler, A. Kaya, M. Weber, *J. Vac. Sci. Technol. B* **1996**, *14*, 4105.
[10] C. Schössler, H. W. P. Koops, *J. Vac. Sci. Technol. B* **1997**, *16*, 862.
[11] C. Schössler, J. Urban, H. W. P. Koops, *J. Vac. Sci. Technol. B* **1997**, *15*, 1535.
[12] S. M. Sze, *Physics of Semiconductor Devices*, 2nd ed., Wiley, New York **1981**.
[13] W. H. Brattain, J. Bardeen, *Bell Syst. Tech. J.* **1953**, *32*, 1.
[14] P. S. Plekhanov, T. Y. Tan, *Appl. Phys. Lett.* **2000**, *76*, 3777.
[15] R. G. Forbes, *J. Vac. Sci. Technol. B* **1999**, *12*, 526.
[16] A. A. G. Driskill-Smith, D. G. Hasko, H. Ahmed, *Appl. Phys. Lett.* **1999**, *75*, 2845.
[17] K. L. Jensen, M. A. Kodis, R. A. Murphy, E. G. Zaidman, *J. Appl. Phys.* **1997**, *82*, 845.

Metallodielectric Photonic Crystals Based on Diblock Copolymers**

By *Michael Bockstaller*, *Rainer Kolb*, and *Edwin L. Thomas**

Propagation of light inside a material is intimately linked with the response of the material to optical stimulus. The interaction between the optical field and the material is represented by the index of refraction. Photonic crystals are structures in which the refractive index is a periodic function of space. In a periodic refractive index structure, forbidden frequency bands can occur for electromagnetic waves. These photonic bandgaps are due to the interference of waves, which experience multiple scattering by an ordered system of scatterers. Photonic bandgap materials facilitate the coherent localization of light, which has resulted in novel quantum optical phenomena as well as important technological applications such as zero threshold microlasers, single-mode light-emitting diodes (LEDs), and all-optical transistors.[1–5]

The realization of photonic crystals for optical or near infrared (IR) frequencies is still a major technological challenge requiring new approaches for refractive index engineering. Whereas most of the current work is performed by lithographic methods, self-assembling structures hold the promise of relatively inexpensive, large-sized photonic bandgap materials in the visible and near IR. Based on this idea a lot of work has been performed using self-assembled colloidal crystal structures.[6,7] Colloidal crystals, however, are rather sensitive to crystallization conditions, which may require long timescales, and in general exhibit a significant amount of inherent disorder and their mechanical properties are rather poor. Fink et al.[8] introduced the idea of using self-assembled diblock copolymer structures as photonic materials. Diblock copolymers consist of chemically different macromolecules, or blocks, joined at their endpoints to form a chain. Due to the positive free energy of mixing of the A and B species the respective blocks tend to segregate. Being restricted by their connectivity, diblock copolymers tend to segregate into microdomains that are of the length scales of the respective blocks. The large number of block compositions and block arrangements lead to a wealth of morphologies, which can in turn provide a set of interesting material templates for photonic applications. Unfortunately, because of the low dielectric contrast in virtually all block copoly-

[*] Prof. E. L. Thomas, M. Bockstaller
Department of Materials Science and Engineering, M.I.T.
Cambridge, MA 02139 (USA)
E-mail: elt@mit.edu
R. Kolb
Corporate Strategic Labs., ExxonMobil R&D
1545 Route 22 East, Annandale, NJ 08801 (USA)

[**] The authors acknowledge Thomas Wagner at the Max Planck Institute for Polymer Research in Mainz, Germany, for his help with anionic polymerization of thiol-terminated poly(styrene). The authors also acknowledge the help of Peter de Rege, M.I.T. with the synthesis of the PS-*b*-PE/P diblock copolymer. Financial support of the Alexander von Humboldt foundation and Nanovation Technologies is gratefully acknowledged.

  0935-9648/01/2312-1783 $ 17.50+.50/0